

MOX–Report No. 19/2011

**An Integrated Statistical Investigation of the Internal
Carotid Arteries hosting Cerebral Aneurysms**

PASSERINI, T.; SANGALLI, L.; VANTINI, S.;
PICCINELLI, M.; BACIGALUPPI, S.; ANTIGA, L.;
BOCCARDI, E.; SECCHI, P.; VENEZIANI, A.

MOX, Dipartimento di Matematica “F. Brioschi”
Politecnico di Milano, Via Bonardi 9 - 20133 Milano (Italy)

mox@mate.polimi.it

<http://mox.polimi.it>

An Integrated Statistical Investigation of the Internal Carotid Arteries hosting Cerebral Aneurysms

Tiziano Passerini · Laura M. Sangalli ·
Simone Vantini · Marina Piccinelli · Susanna
Bacigaluppi · Luca Antiga · Edoardo
Boccardi · Piercesare Secchi · Alessandro
Veneziani

Abstract Cerebral aneurysm formation is the result of a complex interplay of systemic and local factors. Among the latter, the role of the geometry of the vessel hosting an aneurysm (parent vessel) and the induced hemodynamics still needs to be carefully investigated. In this paper we have considered a data set of 52 patients, reconstructed the geometries of the parent vessel and extracted the relevant morphological features with image processing methods. We performed the computational fluid dynamics analysis of these patients with a finite element solver. We have collected in this way a set of data including morphology and wall shear stress along the parent vessel. Thanks to a functional principal component analysis we related relevant

This work has been supported by the Foundation Politecnico di Milano with SIEMENS Medical Solutions Italy (ANEURISK Project), the Brain Aneurysm Foundation “Computational and Statistical Analysis of Brain Aneurysm Morphology & Hemodynamics and the Italian MIUR FIRB research project “Advanced statistical and numerical methods for the analysis of high dimensional functional data in life sciences and engineering”.

T. Passerini, M. Piccinelli, A. Veneziani
Department of Mathematics and Computer Science, Emory University
Tel.: +1-404-7277925
E-mail: tiziano,marina,ale@mathcs.emory.edu

L. M. Sangalli, S. Vantini, P. Secchi
MOX (Modeling and Scientific Computing, Department of Mathematics, Politecnico di Milano, E-mail:
laura.sangalli,simone.vantini,piercesare.secchi@polimi.it

S. Bacigaluppi
Department of Neurosurgery, Niguarda Ca'Granda Hospital, Milan, Department of Neurosciences
and Biomedical Technologies, University of Milano-Bicocca, Monza, Italy E-mail: susannabaci-
galuppi@yahoo.it

L. Antiga
Orobix, Bergamo, Italy
E-mail: luca.antiga@gmail.com

E. Boccardi
Department of Neuroradiology, Niguarda Ca Granda Hospital, Milan
E-mail: Edoardo.Boccardi@OspedaleNiguarda.it

geometrical and fluid dynamical features to a classification of patients depending on the location of the aneurysms and the rupture status. This analysis is anticipated to provide a contribution for the assessment of an index for the rupture risk.

Keywords Cerebral Aneurysms · Image Processing · Computational Fluid Dynamics · Functional Principal Component Analysis

Mathematics Subject Classification (2010) 92C35 · 76Z05 · 65M60 · 60G20 · 62M30

1 Introduction

Cerebral aneurysms formation is considered the result of the complex interplay among systemic effects, the biomechanical properties of the vessel wall and the continuous effect of forces exerted by blood flow on the vessels [16,23,10,35].

While systemic factors influencing the development of the pathology such as genetic conditions, smoking, hypertension and familial predisposition affect the whole arterial vasculature, cerebral aneurysms tend to occur in regions with particular features such as bends and bifurcation apexes. This clinical evidence supports the hypothesis of a major involvement of hemodynamics in the aneurysms pathophysiology.

However the underlying mechanisms triggering the onset of the disease still need to be identified and explained, as well as the specific factors causing some lesions to rupture rather than others. This is a particularly challenging task, given the inter-individual variability of the cerebro-vascular districts, the simultaneous presence of different relevant factors and the difficulty of collecting crucial information, in particular of follow up observational studies that could provide insights to the history of unruptured aneurysms. On the other hand the accomplishment of this task would result in the definition of reliable rupture risk indexes, that would potentially provide a mean to stratify aneurysms according to their probability of bleeding and support clinicians in the critical management of unruptured lesions.

In the last decades the focus of computational fluid dynamics (CFD) studies has mainly concentrated on the intra-aneurysmal flow features and wall shear stress distributions on the sac dome [11,35,12,19] and on the extraction of morphological indexes of aneurysmal sac shape and size [28,13,36]. Recently some authors have underlined the importance of the modeling and characterization of aneurysm parent vasculature. Castro et al [9] studied the influence on intra-aneurysmal flow of the portion of the upstream parent vessels included in the computational domain; Imai et al [18] and Sato et al [34] demonstrated by means of parametric studies on idealized models that different degrees of torsion of the feeding artery remarkably affect inflow patterns and flux; Hoi et al [17] parametrically studied the effect of the parent artery curvature and found that flow impingement area linearly intensifies with the parent artery curvature. An image-based detailed analysis of the geometric features of the internal carotid artery related to the location and rupture of lateral aneurysms has been carried out by Piccinelli et al in [25], which is the observational study that has driven the present work.

Nevertheless, investigations on the relationship between three dimensional (3D) morphology of patient-specific vasculature and hemodynamics still have to face many challenges: primarily, real anatomies display very large variability, especially in the intracranial vasculature, and the retrieval of 3D geometric features in a robust and operator-independent way is a developing but not yet established field; secondly, a quantitative analysis of integrated datasets including geometric information and hemodynamics results, is to the authors' knowledge a rather new field that requires the application and development of ad hoc tools.

This paper aims at giving a contribution in this direction with two distinctive features, one refers to the specific subject of our investigation, the other one to the methods adopted for the data analysis.

1. The focus of our study is the quantitative and computational characterization of the geometry and hemodynamics of the Internal Carotid Artery (ICA) comparing features of those harboring aneurysms, with those with aneurysms in a downstream location (or no aneurysms at all). Vessel geometry has been recognized as a relevant factor in vascular pathologies since a long time, but a precise and quantitative analysis of the geometry of intracranial arteries as preferred sites of development of aneurysms is still insufficient (see [25]). Analogously, CFD studies usually focus on aneurysmal flow rather than on a characterization of the feeding arteries. The vessel geometry is here characterized by means of radius and curvature, while wall shear stress (WSS), its axial gradient and blood energy drop along the ICA path are considered as compact measures of hemodynamics features.
2. Heterogeneity and variability of the data at hand demand for sophisticated statistical methods. Our dataset comprises both geometry and fluid dynamics: these quantities are regarded as stochastic functions of an axial coordinate defined along the vessel. To extract patterns from such a complex aggregate of information we resorted to advanced statistical techniques, namely the *Functional Principal Component Analysis* (FPCA). These methods would allow to identify the part of the data set relevant for our purposes, i.e. the detection of recurrent patterns in geometry and/or fluid dynamics that may relate to the presence of the pathology and a lesion rupture event.

The main methodologies employed in this work have been presented in a series of papers [31,30,26,25] written within the collaborative framework of the *Aneurisk* project and to which we will refer for technical details. *Aneurisk* (2005-2008) was a research project including academic and non-academic groups in the Milan area in Italy¹ whose goal was the development of a framework for the study of cerebral aneurysms. It was based on the idea of integration of different types of information - from the radiological acquisition, to the 3D reconstruction of patient-specific anatomies and their geometric characterization, the CFD modeling and the statistical

¹ Partners of *Aneurisk*: MOX - Department of Mathematics, Politecnico di Milano (PI institution), M. Negri Institute, Bergamo, Department of Neurosurgery, Niguarda Ca'Granda Hospital, Milan, Department of Neurosciences, University of Milan, LABS - Department of Civil Engineering, Politecnico di Milano; Support: Fondazione Politecnico di Milano, SIEMENS Medical Solutions.

analysis of the comprehensive dataset - in order to devise rupture risk indexes with diagnostic and possibly prognostic purposes.

The paper is organized as follows. In Sect. 2 the three components of our methodological workflow are presented: the reconstruction of 3D models and their geometric characterization, the CFD modeling and the Statistical tools employed. Sect. 3 illustrates the results obtained after the statistical analysis. A phenomenological discussion of the results is carried out in Sect. 4.

2 Materials and Methods

2.1 The Data Set

Between September 2002 and September 2006, 65 patients underwent 3D-RA for cerebral aneurysm assessment following clinical routine at the Neuroradiology Division of the Niguarda Ca', Granda Hospital in Milan. Acquisitions were performed with an Integris Allura Unit (Philips, Best, the Netherlands) with the following parameters: C-arm rotation speed, 55 per second; matrix size 512x512; frame rate, 25 frames per second; 18 mL nonionic hydrosoluble contrast agent was injected prior to the acquisition at 4mL/s. The rupture status of the aneurysms was kept for our records. The radiological images were subsequently collected in DICOM format and made available for successive processing and analysis.

In the present study, the original data set has been reduced to 52 patients, since some patients were presenting general conditions (e.g. local stenosis, dysplasia, etc.) unsuitable for the fluid dynamics analysis.

The patients were subdivided into groups according to the location and the rupture status of the lesions. More precisely, we distinguished preliminary two classes of patients

Upper group: subjects with an aneurysm at the terminal bifurcation of the ICA or after it;

Lower group: subjects with an aneurysm along the ICA, before its terminal bifurcation or subjects without aneurysms.

In this paper we refer to a more refined classification, including the rupture of the aneurysm. More precisely we considered 5 classes,

UR (Upper Ruptured): subjects with a ruptured aneurysm at or after the final bifurcation of the ICA;

UN (Upper Non-ruptured): subjects with a non-ruptured aneurysm at or after the final bifurcation of the ICA;

LR (Lower Ruptured): subjects with a ruptured aneurysm along the ICA, before its terminal bifurcation;

LN (Lower Non-ruptured): subjects with a non-ruptured aneurysm along the ICA, before its terminal bifurcation;

No (No Aneurysm).

Table 1 reports the size of each group, demographic information about the patients, as well as details on the localization of the lesions within each subclass.

Group	Size	Position			
		ICA	MCA	ACA	
U	UN	11	1	5	5
	UR	16	1	2	13
L	LN	13	13	0	0
	LR	9	9	0	0
No	3	0	0	0	
Total	52	24	7	18	

Table 1 Summary of the Aneurisk data set considered in the present study. For the explanation of the classes, see Sect. 2.3.1.

2.2 The workflow: geometric characterization

The reconstruction of patient-specific anatomies and part of the geometric characterization of the parent vasculature were achieved by means of the Vascular Modeling Toolkit (VMTK) [3].

More in details, the following operations were performed for each patient.

1. The 3D surface model of the aneurysm and its parent vessels was reconstructed by means of a gradient-driven level-set approach [5]; in particular all the acquired portion of parent vasculature was included in the model.
2. The centerlines of the reconstructed vascular network were extracted [6] as well as a centerline traveling through the aneurysm sac, as described in [25]; a point-wise estimate of the vessels radius was readily available from the centerline computation techniques [26].
3. According to methodologies described in [26] the vascular network bifurcations were automatically identified and the centerlines accordingly tagged for each vascular branch; the same subdivision was successively applied to the 3D surface model.
4. A curvilinear abscissa was defined travelling along the vessel: selecting the ICA bifurcation [26] as a landmark on all the models, the abscissa robustly measured and parameterized the ICA length in the upstream direction; by definition *the abscissa was zero at the bifurcation point and assumed negative values moving upstream* (for this reason the subsequent diagrams will present negative values of the abscissa) .

As a consequence of these splitting procedures, the parent artery geometry and morphological features were automatically extracted from the complete 3D model and made available for successive investigations.

For one of the analyzed cases Figure 1 illustrates the geometric characterization performed, the 3D modeling, the split centerlines network and the corresponding subdivided surface.

2.3 The workflow: CFD

The region of interest represents the siphon of the ICA and its main bifurcation: starting from the 3D model, the ICA was kept entirely while the downstream circu-

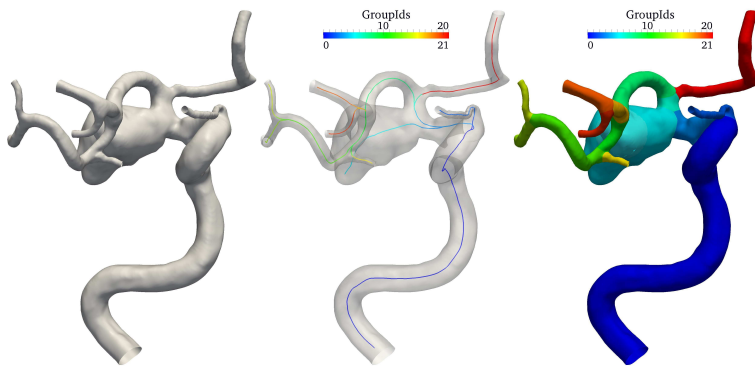


Fig. 1 Left: 3D surface model of ICA hosting an aneurysm; middle: split centerlines for the whole vascular network; right: split 3D surface model.

lation was properly trimmed. Cylindrical prolongations (*flow extensions*) were added at each extremal section of the surface, in such a way that the geometrical model featured circular inlet and outlet sections, corresponding to the proximal and the distal boundaries respectively. The length of these cylindrical extensions was adaptively selected as 10 times the clipped section radius.

For each geometrical model we obtained a tetrahedral grid with an average element size of 0.06 cm using the Netgen Mesh Generator. The computational domain was assumed to be fixed, corresponding to the hypothesis of rigid vascular walls. We further assumed that blood can be modeled as a continuous incompressible Newtonian fluid, so that the blood flow problem can be described by the incompressible Navier-Stokes equations (see e.g. [14]). For each vascular geometry, three cardiac cycles were simulated, in order to reduce the effects of the initial conditions and obtain the periodic solution in the last simulated heartbeat.

The spatial discretization was based on the Galerkin finite element method, and was carried out with a piecewise linear approximation for both the pressure and the velocity. The numerical scheme adopted is based on an edge stabilization technique [8] that allows to use this kind of approximation. The adopted time advancing scheme is a semi-implicit Euler method, with a time step of 10^{-3} s.

To estimate the stress field (and in particular the wall shear stress) over the computational domain it is necessary to retrieve a suitable approximation of the velocity gradient. We used an L^2 *projection method* [37, 7], which is proven to provide a superconvergent approximation of the gradient on linear elements.

In the Aneurisk dataset, patient-specific measurements of blood flow rates, velocity or pressures were unfortunately not available, since their routine acquisition is not in the approved protocol. On the other hand, physiological values for ICA flow rate can be found in the literature. Since our interest was to compare different vascular geometries, and to understand the effect of different morphological features on hemodynamics, starting from the available data we looked for a suitable set of boundary conditions for our geometrical models. We prescribed boundary conditions giving the same flow regime in all the computational domains. More precisely, as a descriptor of the flow regime, we adopted the time average Reynolds number, evaluated on the

inlet section. For the models at hand, a time average Reynolds number of $Re = 350$ was found to describe with a good approximation the flow regime associated to an ICA flow rate in the range of physiological values [24]. Therefore, we scaled the amplitude of the inflow datum to obtain that value in each geometry.

The chosen flow rate was obtained by prescribing a velocity profile on the inlet section, more precisely a flat axial velocity profile. This choice is legitimated by the use of a cylindrical boundary extension on the inlet section. It is indeed proven that the geometrical features of the vessel have a stronger influence on the solution than the presence of secondary velocities in the inlet profile [15, 22]. Moreover, the effects of inlet secondary flows, even in case they are present, break down within a few diameters of the inlet [21].

In order to include the WSS and its gradient into the integrated morphology-fluid dynamics analysis, we computed a one dimensional function depending on the position along the curvilinear abscissa. As a matter of fact, let \mathbf{T} denote the stress tensor of the fluid,

$$\mathbf{T} = -p\mathbf{I} + \mu(\nabla\mathbf{u} + \nabla\mathbf{u}^T)$$

where p is the pressure, \mathbf{u} the velocity and μ the dynamic viscosity. The WSS of patient i is then a vector field tangential to the wall defined as

$$\text{WSS}_i(x, y, z, t) = \mathbf{T} \cdot \mathbf{n} - (\mathbf{n} \cdot \mathbf{T} \cdot \mathbf{n})\mathbf{n}$$

where \mathbf{n} denotes the unit normal vector to the wall and we explicitly express the dependence on the spatial coordinates x, y, z and on time t . The parent vessel is subdivided into a sequence of sections located at the curvilinear abscissas s_k such that $s_{k+1} - s_k = 2\text{mm}$ (see Fig. 2). Each section is taken orthogonal to the centerline and is corresponded by a slice \mathcal{S}_k of the surface of the vessel (represented on the left with different colors as a function of s_k). The slices are non overlapping, and their boundaries are defined by edges of the computational grid.

We then compute the magnitude of the average WSS on the slice \mathcal{S}_k , so that we define the local average WSS as a function of s_k and time

$$\overline{\text{WSS}}_i(s_k, t) = \left\| \frac{1}{|\mathcal{S}_k|} \int_{\mathcal{S}_k} \text{WSS}_i(x, y, z, t) d\mathcal{S} \right\|.$$

The value $\overline{\text{WSS}}_i(s_k, t_{\text{sys}})$ assumed at the systolic peak was taken as the one dimensional fluid dynamics indicator together with the axial derivative $\frac{d\overline{\text{WSS}}_i}{ds}(s_k, t_{\text{sys}})$. They are actually functions of the curvilinear abscissa, as are radius and curvature of the vessel centerline. Therefore, they can be treated with the same tools in the statistical analysis, as detailed in following sections.

For the discussion that follows we need also to quantify the energy loss experienced by the blood stream when flowing through the ICA. This is estimated by computing the difference of the total mechanical energy of the fluid on two cross-sections of the vessel, located upstream (*Section U*) and downstream (*Section D*) the siphon. In all the geometries, the downstream section was located at the terminal bifurcation of the ICA. The upstream section was located at the most proximal location available in all the considered geometries, after alignment of the vessels centerlines

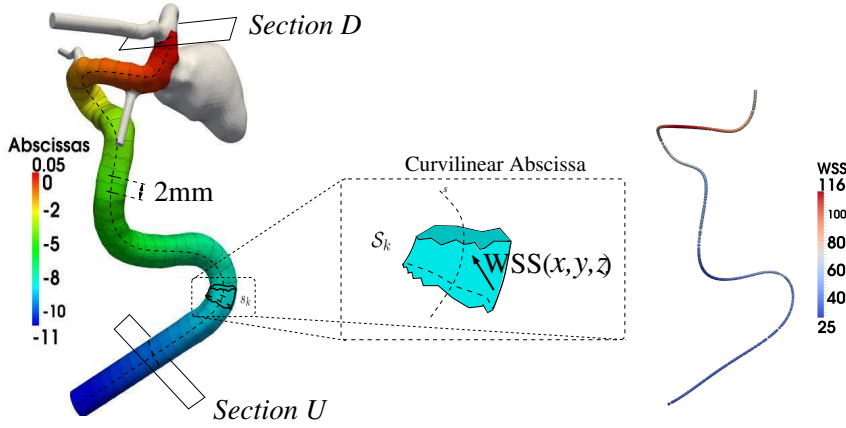


Fig. 2 Computation of the average shear stress $\overline{\text{WSS}}$ as a function of the curvilinear abscissa s . Left: the vascular surface is subdivided in slices \mathcal{S}_k , corresponding to a set of equispaced values of the curvilinear abscissas (the width of the step is 2 mm). Right: the averaged shear stress is associated to centerline points.

as detailed in the following. The total mechanical energy is defined as the sum of the kinetic, potential, and flow energies of the fluid. In the system at hand the variation in potential energy was negligible due to the small differences in height of the sections of interest, therefore the energy loss (per unit volume) was computed as

$$\mathcal{L}(t) = \int_{\text{SectionD}} \left(\rho \frac{\mathbf{u} \cdot \mathbf{u}}{2}(t) + p(t) \right) ds - \int_{\text{SectionU}} \left(\rho \frac{\mathbf{u} \cdot \mathbf{u}}{2}(t) + p(t) \right) ds$$

where ρ is the fluid density. The quantity \mathcal{L} was computed at each time step of the simulation, and averaged over the cardiac cycle with duration T , so that we refer to

$$\overline{\mathcal{L}} = \frac{1}{T} \int_0^T \mathcal{L}(t) dt.$$

For a periodic viscous flow, this yields the estimation of the viscous dissipations.

2.3.1 The workflow: Data analysis

The analysis of the data reconstructed from the geometry required three main steps.

1. functional representation of the centerlines (approximation) and its differentiation;
2. alignment of the centerlines (registration);
3. identification of the relevant information (functional principal component analysis - FPCA) and discriminant analysis.

In the first step we approximate with a smooth function the centerlines of each internal carotid artery (ICA) reconstructed by VMTK. After the reconstruction, in fact, we have a pointwise representation of the lines in terms of nodes P_k with coordinates (x_k, y_k, z_k) where k ranges from 0 to an appropriate number of points. Since we are

interested in the curvature of the centerline, requiring the differentiation of a parametric representation of the centerline, a piecewise linear interpolation is inadequate. Among different strategies, we resorted in [31] to a functional representation based on *free-knots splines* of order 4. This corresponds to a piecewise polynomial approximation where the knots separating each polynomial are not selected *a priori*. They are actually selected for obtaining a simultaneous minimization of the approximation error (in the least square sense) and of the number of knots itself.

The top left panel of Figure 3 shows the derivatives of the three space coordinates of the estimated ICA centerlines, $\{x'(s), y'(s), z'(s)\}$, for each subject along the curvilinear abscissa. This quantities well represent the variability of our data set. What is evident from the figure (referring to the reduced data set of 52 patients of this paper) is a remarkable misalignment of the data. In particular we noticed a strong phase variability largely due to the different size of the body and thus of the arteries of the different patients. To filter this effect out we decoupled the *phase variability* among the subjects, strongly dependent on ICAs dimensions, from an *amplitude variability*. The latter reflects actually the variability in the morphological shapes of ICAs, in which we are mostly interested. In [30] we described a technique that is able to decouple the two types of variability, providing the aligned centerlines displayed in the right panel of Figure 3, that can thus be profitably used for comparisons across subjects. The template resulting from the comparison of the different subjects is reported in the pictures as a black bold line. In fact, even after alignment, the centerline first derivatives displayed in Figure 3 show a large phase variability, especially at values of the abscissa between -50 and -20mm. This suggested the presence of more than one prototype morphological shape of ICAs.

For this reason, in [33] we proposed a procedure that is able to jointly align and cluster a set of curves in multiple groups. We tested in particular a grouping based on the assumption of k clusters, with $k = 1, 2, 3$, as depicted in Fig. 4, left. The significance of the similarity among individuals of the same cluster was largely improved by the alignment. Moreover, left panel of Fig. 4 pinpoints that the level of similarity is not significantly improved when passing from 2 to 3 clusters. For this reason we eventually concluded that two clusters (with the two corresponding templates) are an accurate representation of the data set. The mean curves of the two cluster are reported in Fig. 4, right. The two mean centerlines identified in this way are represented in 3D in Fig. 5.

The two estimated templates identify two prototype morphological shapes of ICA that have since long time been described in medical literature [20]. Namely, the green template centerline is a prototype of a so-called Ω -shaped ICA, whose siphon has just one main bend in its distal part; the orange one is instead a prototype of a so-called S-shaped ICA, whose siphon has two main bends in the distal part. The analysis in [33] on the larger data set of 65 subjects showed that the allocation of a subject into the Ω -shaped ICAs and S-shaped ICAs clusters is correlated to different settings of aneurysm development (Table 2).

Given the alignment of the curve, all the data associated with the centerlines (radius, curvature, $\overline{WSS}(s, t_{sys})$, etc.) have been registered accordingly. After the geometrical reconstruction, the approximation and the alignment steps, for each patient we had a set of three functions representing each variable of interest as a function of the

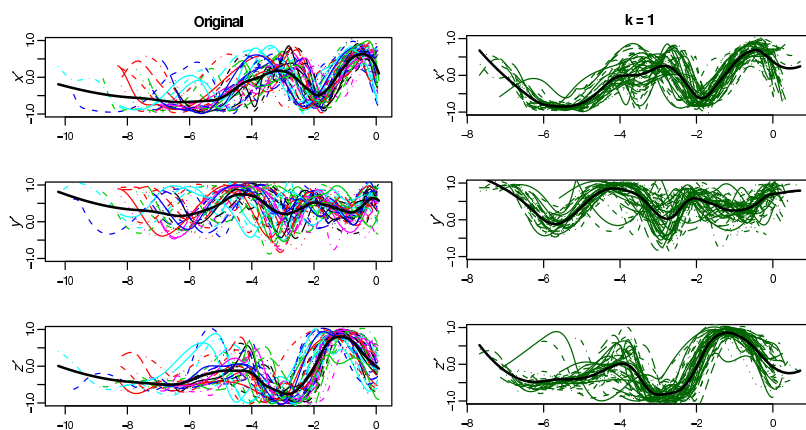


Fig. 3 Left: first derivatives with respect to the curvilinear abscissa of the centerlines coordinates ($x' = dx/ds, y' = dy/ds, z' = dz/ds$) of the estimated ICA, reconstructed from images after the free knot interpolation. The black thick curve represents the template reconstructed by the data without alignment. Right: first derivatives of centerlines after the alignment. We identified here just one cluster of data ($k = 1$). The template of this cluster is represented again by the black thick line.

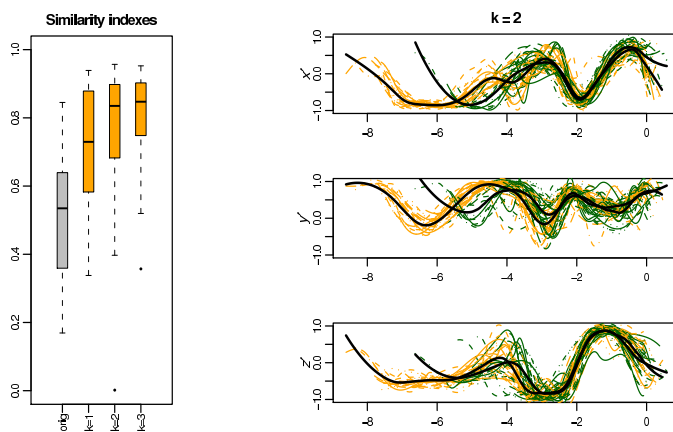


Fig. 4 Left: boxplots of similarity indexes between each curve and the corresponding template for original estimated centerlines and for centerlines aligned and clustered in k groups, $k = 1, 2, 3$. Right: After the alignment, a better clustering is obtained with two groups ($k = 2$), whose templates are represented by the solid thick lines.

Position	at/after ICA bifurcation	along ICA	No aneurysm
Ω	70%	48%	0%
S	30%	52%	100%

Table 2 Conditional contingency table of subjects allocations to Ω -shaped ICAs and S-shaped ICAs clusters.

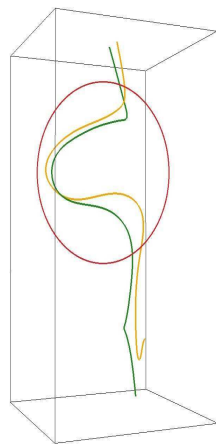


Fig. 5 3D image of the estimated templates of the two clusters. The green template is a prototype of Ω -shaped ICA (single-bend siphon), the orange one is a prototype of S -shaped ICA (double-bend siphons).

registered curvilinear abscissa s along the centerline. These functions are regarded as the realization of a random function, whose features could be significantly correlated to the belonging of the subject to a specific group. The identification of such features is however made difficult by the huge complexity of the data represented by these functions. *Functional Principal Component Analysis* (FPCA) pursues the goal of a reduction of the complexity of the data. Similarly to a modal decomposition, FPCA aims at identifying a finite dimensional subspace onto which to project the functional data providing a good compromise between information loss and statistical power gain (Karhunen-Loève decomposition of the sample autocovariance operator). The identification of the most convenient basis (the set of *principal components*) for representing the stochastic functions at hand is data driven: FPCA actually identifies important and uncorrelated modes of variability observed in the data set i.e., sample autocovariance operator eigenfunctions. The coordinates of the projections of the data onto the modes in the basis are called *scores*. The statistical relevance of the modes in the basis can be quantified by means of the sample variance of the scores of the projected data i.e., sample autocovariance operator eigenvalues. Once dimensional reduction has been achieved, classical multivariate analysis of the scores of the principal components is used to investigate and verify the statistical hypothesis of interest. For an extensive introduction to these techniques we refer to [29].

In particular, we looked for patterns that discriminate patients in different classes. Discrimination was carried out by an approach called *Quadratic Discriminant Analysis* (QDA), which is a classification rule assuming, for each investigated class, a multivariate Gaussian distribution of the observed features. The basic idea is to calculate the relative proportions of the classes, their means and their covariance matrices with respect to the variables analysed. For each possible set of features presented by a new subject, Bayes Theorem provides an estimate of his probability of belonging to each one of the groups.

Results of the combined FPCA+QDA analysis on the enriched (geometry + CFD) data set with respect to the classification presented in Table 1 are presented in the next section.

2.4 Software

We summarize here the software packages used and partially developed within the framework of the present research.

1. *Vascular Modeling ToolKit* (VMTK) [3] is an open-source project for 3D segmentation, geometric analysis, mesh generation and surface data analysis for image-based modeling of blood vessels. The code is downloadable at www.vmtk.org.
2. *LifeV* is a software project born from the joint collaboration of three institutions: École Polytechnique Fédérale de Lausanne (CMCS) in Switzerland, Politecnico di Milano (MOX) in Italy and INRIA (REO) in France. The Department of Mathematics and Computer Science of Emory University in Georgia (USA) started a collaboration since 2008. LifeV consists of the implementation in C++ language of algorithms and data structures for the numerical solution of partial differential equations. The library has been recently extended with the support for parallel computing. The source code is publicly available for download at www.lifev.org.

We also used the following external packages.

1. *NetGen* for the generation of computational grids [1].
2. *Paraview* for the preparation of the vascular geometries and the visualization of the CFD results [2].
3. The statistical analyses have been carried out within the statistical programming environment *R* [27].

3 Results

In order to analyze the morphological and hemodynamical features relevant for the position of the aneurysm and the rupture status, in [30] we have investigated the functions $R_i(s)$ and $C_i(s)$ corresponding to ICA radius and curvature of the patient i . We showed that subjects in the Upper group have wider and more tapered ICAs than those in the lower group, with a less curved ICA. Moreover, ICA radius and curvature profiles have a significantly lower variability among Upper group subjects than among Lower group subjects, so that the former are very well characterized by these two geometric features [30].

In order to improve this analysis and correlate the results with the rupture, we expanded the analysis with the data coming from the CFD.

In Fig. 6 ICA radius and curvature, and the local average \overline{WSS} are presented as functions of the curvilinear abscissa on the centerline. The figure shows the large variability of the data set, even after centerline alignment. It is worth noting that the length of the reconstructed centerlines has also a great variability in the data set. This

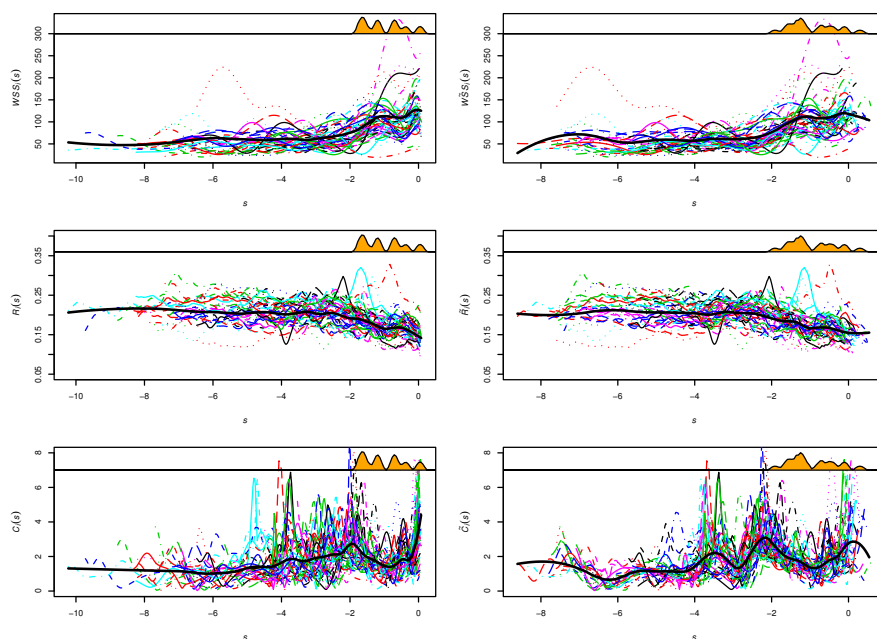


Fig. 6 ICAs \overline{WSS} (top), radius (center) and curvature (bottom) profiles for all subjects respectively before (left) and after (right) registration. Solid black lines show mean curves, as estimated by Loess. On top of each picture is also displayed the estimate of the probability density function of the location of aneurysms along the ICA or at its terminal bifurcation.

figure also displays, at the top of each plot, a Gaussian kernel estimate of the probability density function of the location of aneurysms along the ICA or at its terminal bifurcation. Occurrence of the aneurysms in the distal part of the ICA (where tapering is more evident), is almost null at $s \approx -1$ cm. This indirectly identifies the average position of the dural ring the ICA goes through before its terminal bifurcation. Notice that the dural ring is not detectable from images and that aneurysms distal to this position are in general more life threatening.

In this study we concentrated on the distal ICA, comprising the last 5 cm before its terminal bifurcation, given that this was the available tract in all considered patient's 3D models after centerline registration.

A representative subject for each class of Tab. 1 is presented in Figures 7-11. On the left column we show the 3D model of the Internal Carotid Artery, as defined after reconstruction from images and mesh generation. The magnitude of the computed WSS vector at the systolic peak is plotted on the vascular surface. On the right column we show the morphological and hemodynamical indices evaluated on each subject, expressed as functions of the curvilinear abscissa along the vessel centerline. This sequence of figures highlights the most relevant differences of ICAs in the different groups, by direct comparison.

Notice that only the subject in the LR group presents an abrupt change of the \overline{WSS} values along the centerline curvilinear abscissa (Fig 9) located at the distal half of the

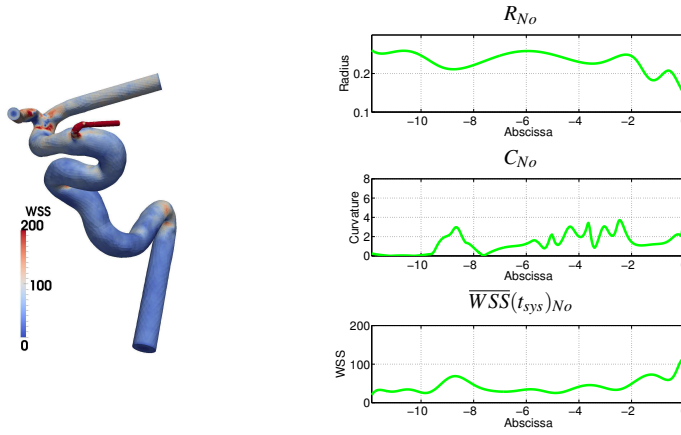


Fig. 7 Representative of group No: the \overline{WSS} at the systolic peak (left); The radius (cm), curvature (cm^{-1}) and $\overline{WSS}(t_{\text{sys}})$ at the systolic peak as functions of the curvilinear abscissa (right).

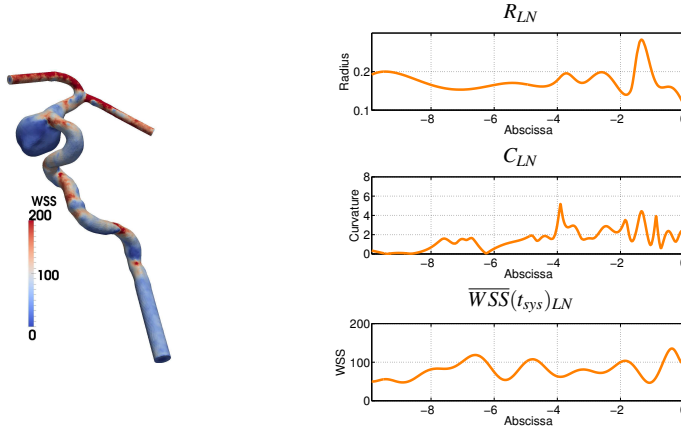


Fig. 8 Representative of group LN: the \overline{WSS} at the systolic peak (left); The radius (cm), curvature (cm^{-1}) and $\overline{WSS}(t_{\text{sys}})$ at the systolic peak as functions of the curvilinear abscissa (right).

$\overline{\mathcal{L}}$ (mmHg)	No	LN	LR	UN	UR
	4.47	5.4	4.5	2.74	3.26

Table 3 Power loss computed in the representative subjects for each group.

main bend. The maximum value of the \overline{WSS} is larger in this case than in all the other considered cases, so we guess that it is a consequence of this particular configuration affecting the blood flow.

The two subjects from the "upper" groups (UN, UR) feature relatively low values of the \overline{WSS} , with no abrupt changes in the space pattern (Figures 8, 9). The radius of the ICA is consistently larger in the two subjects belonging to groups UN and UR than in subjects belonging to the other groups.

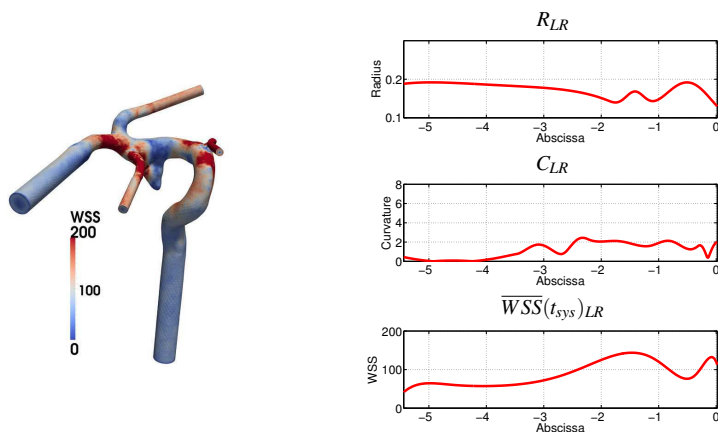


Fig. 9 Representative of group LR: the \overline{WSS} at the systolic peak (left); The radius (cm), curvature (cm^{-1}) and \overline{WSS} (dyn/cm^2) at the systolic peak as functions of the curvilinear abscissa (right).

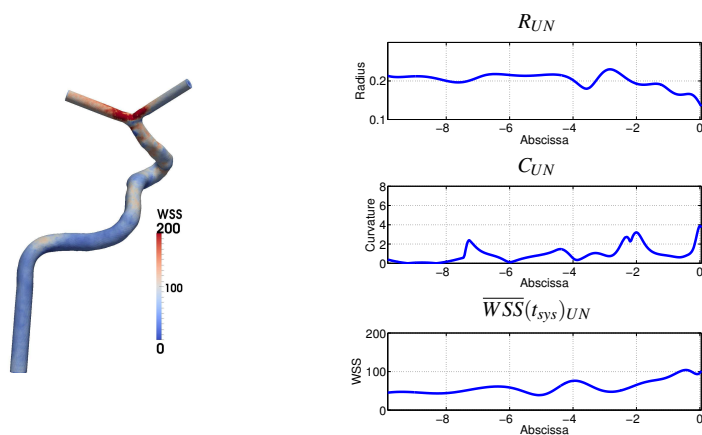


Fig. 10 Representative of group UN: the \overline{WSS} at the systolic peak (left); The radius (cm), curvature (cm^{-1}) and \overline{WSS} (dyn/cm^2) at the systolic peak as functions of the curvilinear abscissa (right).

It is also interesting to notice (see Tab. 3) that the computed energy loss is significantly larger in subjects belonging to the No, LN and LL groups, while subjects in the UN and UR groups feature lower values.

After completing the CFD analysis for all the 52 reconstructed image sets, we separately performed the FPCA of radius, curvature and \overline{WSS} profiles along aligned ICA centerlines, detecting the principal uncorrelated modes of variability of these quantities. This allowed the identification of statistical differences among the five groups of subjects with respect to these modes of variability. In the first row of Fig. 12 we report the profiles of these quantities as a function of the curvilinear abscissa. The second row of the figure displays the projections on the most significant principal components for radius, curvature and \overline{WSS} . Significant differences occur among the five groups of subjects, in particular emphasized by the first principal component

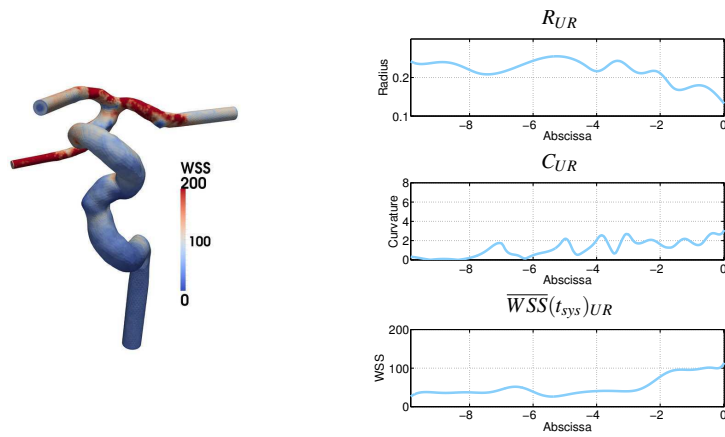


Fig. 11 Representative of group UR: the \overline{WSS} at the systolic peak (left); The radius (cm), curvature (cm^{-1}) and WSS (dyn/cm^2) at the systolic peak as functions of the curvilinear abscissa (right).

of the Radius and the Curvature and the second principal component of the axial derivative of $\overline{WSS}(s, t_{sys})$. The third row of shows the boxplots of the scores of these principal components for the five groups of subjects. p -value in the boxplots is based on the one-sided Wilcoxon test.

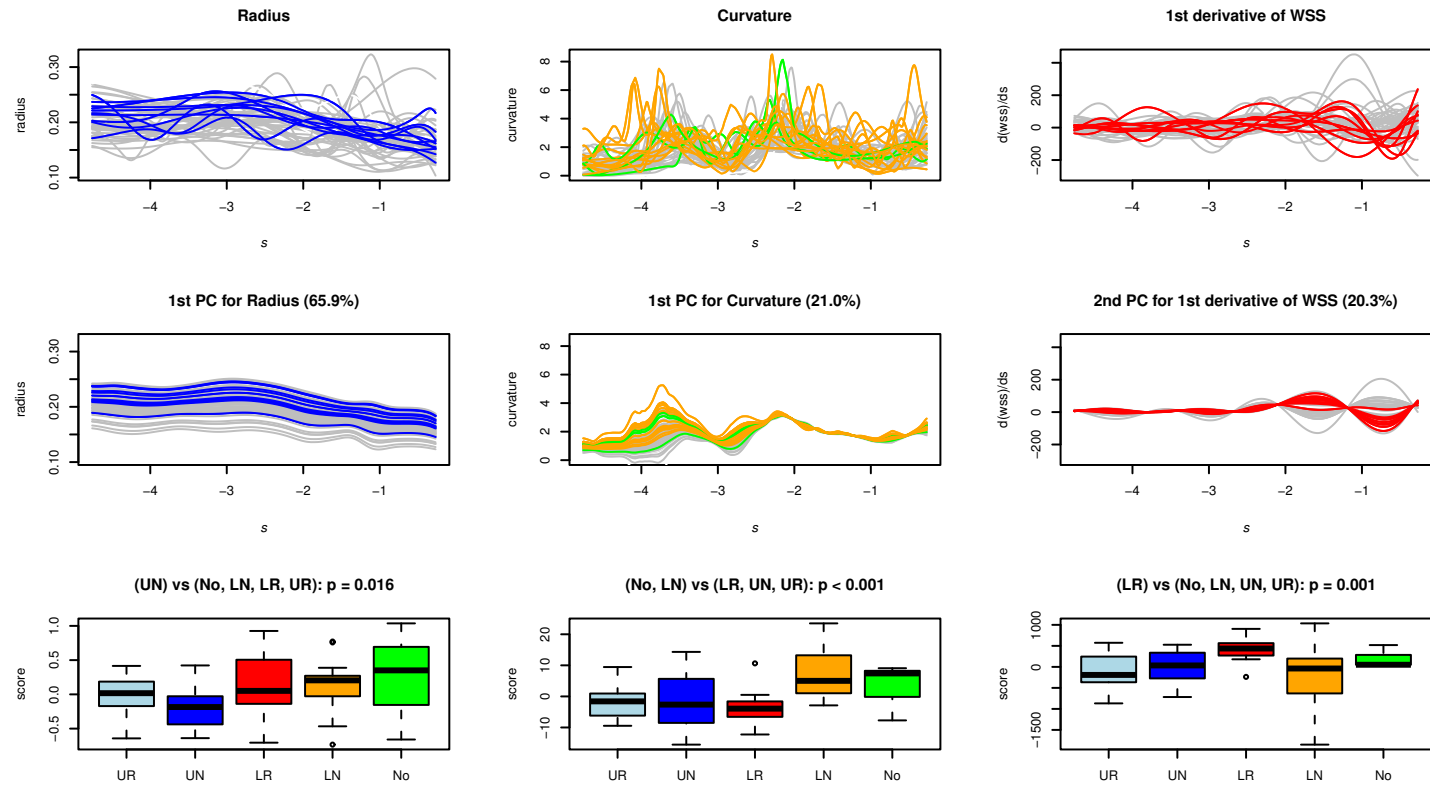


Fig. 12 First column: analysis of ICA radius profiles along aligned centerlines. Second column: analysis of curvature profiles of aligned ICA centerlines. Third column: analysis of the first derivative of the WSS profiles along aligned ICA centerlines. First row: aligned profiles. Second row: projections of subject profiles on the corresponding mode of variability. Third row: boxplots of subject scores on these principal components separated per subject group.

4 Discussion

From the joint morphologic-fluid dynamics analysis, we notice the following facts.

The *first column of Figure 12* shows the projections on the first principal component of the ICA radius profiles along aligned centerlines. For each subject, the component along this mode measures the average radius of the ICA; thus, changing the scores with respect to this mode we move from subjects with a narrow ICA to subjects with a wide ICA. As previously pointed out, in [30] we already highlighted the significance of the width of the ICA in discriminating among Upper and Lower group subjects. With the present analysis we can more specifically notice that **UN** group subjects in particular behave differently from the other four subject groups with respect to this mode of variability, manifesting statistically wider ICAs than other four groups (p -value: 0.016).

The *second column of Figure 12* shows the projections on the first principal component of the curvature profiles of aligned centerlines. For each subject, the component along this mode measures the prominence of the second peak of curvature of the ICA centerline; thus, changing the scores with respect to this mode we move from subjects with a non particularly evident second bend of the siphon to subjects with a very marked one. The significance of the presence/absence of the second bend of the siphon is in accordance to what emerged in [30]. The current analysis refines this result, showing that, the **No** and the **LN** groups seem to behave differently from the other three groups with respect to this mode of variability, being statistically associated to the presence of a double-bend siphon (p -value: ≤ 0.001).

Finally, the *third column of Figure 12* shows the projections on the second principal component of the first (axial) derivative of the WSS profiles along aligned centerlines. For each subject, the component along this mode measures the intensity of the WSS peak at the end of his ICA; thus, changing the scores with respect to this mode we move from subjects with a less pronounced WSS peak to subjects with marked WSS peak. In particular, the **LR** group seems to behave differently from the other four, manifesting statistically more prominent WSS peaks (p -value: 0.001).

The clustering Ω -S, that - as we have pointed out - has been found here on the basis of a purely statistical argument and then matched with the previous literature, seems also relevant for the aneurysm pathology. As a matter of fact, our previous results showed a statistical evidence of a dependence between cluster membership and aneurysm presence and location [32]. In particular the contingency table 2 shows that all the subjects without aneurysms were found to display S-shaped ICAs; at the opposite, among Upper group subjects only a minority had an S-shaped ICA, whilst the majority (70%) had an Ω -shaped one.

Based on these evidences, we formulate the conjecture that the ICA siphon has a protective effect on the intra-cranial arterial tree, with respect to the event of formation of an aneurysm. In fact, most sites of aneurysm development are inside the dura mater, where arteries float in the subarachnoidal space with little or less support from the surrounding tissues, as compared to extradural locations. This could make them more sensitive to the intensity of flow-induced loads, which are dependent on viscous dissipations in the feeding arteries. Viscous dissipations are induced by flow secondary motions that have a complex dependence on the vessel geome-

try [4]. When considering subject-specific arterial geometries, it is hard to identify simple relations between vessel morphology and the hemodynamics, mainly because of the high inter-subject morphology variability. Several geometrical features jointly affect the fluid dynamics. In the case at hand, the curvature of the bends of the ICA siphon is expected to have impact on viscous dissipations. Whilst S-shaped ICAs are expected to be very effective in dissipating the flow energy, Ω -shaped ICAs would not be as efficient. Other features such as the vessel radius will also be relevant, since ICAs featuring larger values of the radius tend to produce less viscous dissipation. Moreover, the fluid secondary motion depends on the torsion of the vessel, in terms of the relative orientation of the subsequent bends.

In the current work, an attempt has been made at selecting a reduced set of indicators, able to capture the relevant features for the classification of the data set. Each indicator alone is providing only a partial characterization of the system at hand. The radius profile is not providing information regarding the shape of the cross section, which can be significantly non-circular as pointed out in [26]. The curvature profile is not providing information about the relative orientation of alternating bends in the siphon. The fluid dynamics indicator is based on arbitrary assumptions on the flow conditions at the boundary of the computational domain. However, the assumptions on the simulated flow conditions are made in order to probe different vascular geometries under the same flow regime. Fluid dynamics is here used as a *proxy* for morphology features which are not easy to be measured or interpreted, and specifically it plays the role of a synthetic descriptor of the effect of secondary motions induced by the vascular morphology. Therefore, the rationale behind the joint evaluation of the three indicators is that under the proposed experimental conditions, information provided by fluid dynamics can complement the morphology characterization of subject-specific vascular structures.

The conjecture on the dissipative role of the siphon is supported by the computed energy loss featured by the blood stream when flowing through the ICA siphon. This value varies across different groups of subjects. Subjects in the No group behave similarly to subjects in the LN and LL groups, whose flow exhibits greater energy loss (or viscous dissipations) in the ICA siphon. The energy loss (Tab. 3) discriminates subjects having an aneurysm in the intra-cranial circulation versus subjects with an aneurysm on the ICA or no aneurysm at all. This is consistent with previous observations in [32] regarding the role of the ICA curvature. However, this result also suggests that energy losses in the ICA cannot be correctly estimated based on the vessel curvature alone. Because of the observational nature of our data, validation and further investigation from a medical point of view is of course needed to thoroughly test this conjecture.

5 Conclusions and Perspectives

There are several limitations in this study. The data set is including 52 patients and the statistical significance of the results would be greatly improved by the extension of the number of patients. We are extending the data set of patients, by including images that will undergo the same procedure. In view of a possible cross validation

of our results and hopefully to corroborate our conclusions, we are preparing a web repository of the geometries considered in the present study. We aim at sharing our data and possibly at receiving more data for incrementing the number of cases of the present analysis.

We have focused the attention on the local average WSS and its axial gradient. These are actually advocated in the literature as principal indicator of different vascular pathologies. However, other indicators could be considered in a similar way, like the Oscillatory Shear Index or the Helicity Factor. On the other hand, it could be interesting to analyse the variation of the local maximum WSS (rather than the local average WSS) as a function of the vessel curvilinear abscissa, to highlight locations that exhibit critical levels of the shear load.

One major improvement of the present study is moreover represented by an integrated analysis of the parent vessel and the sac. The joint analysis of the two regions is anticipated to provide a remarkable insight of the link between the morphology-hemodynamics and the pathology, in particular for a prognostic purpose.

Nevertheless, the results presented here clearly point out that

1. the adoption of sophisticated statistical methods for mining complex and heterogeneous data set can extract significant patterns for a deep comprehension of the pathology;
2. the morphology of the ICA and the consequent blood dynamics is likely to play a significant role in the development (and possibly the rupture) of the aneurysm; the possible role of the siphon in protecting the downstream arterial tree deserves to be further investigated. Since the presence of a pronounced double bend is in general detectable from the images, these results, if confirmed, could improve the prognostic potential of the present analysis.

Disclosure of Potential Conflicts of Interest

All the authors of the present paper declare that they do not have any conflict of interest with the results of the research presented here.

Acknowledgements Laura Sangalli is partially supported by the Italian MIUR FIRB research project “Advanced statistical and numerical methods for the analysis of high dimensional functional data in life sciences and engineering”. Marina Piccinelli, Tiziano Passerini and Alessandro Veneziani acknowledge the support of the Brain Aneurysm Foundation. All the participants acknowledge the support of the Italian Fondazione Politecnico di Milano and the SIEMENS Medical Solutions, Italy. Alessandro Veneziani wishes to thank Dr. Frank Tong (Emory Hospital) for fruitful discussions.

References

1. Netgen Web Site. URL www.netgen.org
2. Paraview Web Site. URL www.paraview.org
3. VMTK software. <http://www.vmtk.org>. URL <http://www.vmtk.org>
4. Abou-Arab, T.W., Aldoss, T.K., Mansour, A.: Pressure drop in alternating curved tubes. *Applied Scientific Research* **48**(1), 1–9 (1991)

5. Antiga, L., Piccinelli, M., Botti, L., Ene-Iordache, B., Remuzzi, A., Steinman, D.: An image-based modeling framework for patient-specific computational hemodynamics. *Medical and Biological Engineering and Computing* **46**(11), 1097–1112 (2008)
6. Antiga, L., Steinman, D.A.: Robust and objective decomposition and mapping of bifurcating vessels. *IEEE Trans Med Imag* **23**, 704–713 (2004)
7. Barlow, J.: Optimal stress location in finite element method. *Int. J. Numer. Methods Eng.* **10**, 243–251 (1976)
8. Burman, E., Fernandez, M., Hansbo, P.: Continuous interior penalty finite element method for Oseen's equations. *SIAM J. Numer. Anal.* **44**, 1248–1274 (2006)
9. Castro, M.A., Putman, C.M., Cebal, J.R.: Patient-specific computational fluid dynamics modeling of anterior communicating artery aneurysms: a study of the sensitivity of intra-aneurysmal flow patterns to flow conditions in the carotid arteries. *AJNR American journal of neuroradiology* **27**, 2061–2068 (2006)
10. Cebal, J., Mut, F., Weir, J., Putman, C.: Association of hemodynamic characteristics and cerebral aneurysm rupture. *American Journal of Neuroradiology* **32**(2), 264–70 (2010)
11. Cebal, J.R., Castro, M.A., Burgess, J.E., Pergolizzi, R.S., Sheridan, M.J., Putman, C.M.: Characterization of cerebral aneurysms for assessing risk of rupture by using patient-specific computational hemodynamics models. *AJNR American journal of neuroradiology* **26**, 2550–2559 (2005)
12. Chien, A., Tateshima, S., Sayre, J., Castro, M., Cebal, J., Viuela, F.: Patient-specific hemodynamic analysis of small internal carotid artery-ophthalmic artery aneurysms. *Surgical Neurology* **72**(5), 444–50 (2009)
13. Dhar, S., Tremmel, M., Mocco, J., Kim, M., Yamamoto, J., Siddiqui, A., Hopkins, L., Meng, H.: Morphology parameters for intracranial aneurysm rupture risk assessment. *Neurosurgery* **63**(2), 185–96 (2008)
14. Formaggia, L., Quarteroni, A., Veneziani, A. (eds.): *Cardiovascular Mathematics*. Springer (2009)
15. Formaggia, L., Quarteroni, A., Veneziani, A.: *Cardiovascular Mathematics*, chap. 11, pp. 401–453. *Modeling, Simulation and Applications*. Springer (2009)
16. van Gijn, J., Kerr, R.S., Rinkel, G.J.: Subarachnoid haemorrhage. *Lancet* **369**(9558), 306–18 (2007)
17. Hoi, Y., Meng, H., Woodward, S., Bendok, B., Hanel, R., Guterman, L., Hopkins, L.: Effects of arterial geometry on aneurysm growth: three-dimensional computational fluid dynamics study. *Journal of Neurosurgery* **101**(4), 676–81 (2004)
18. Imai, Y., Sato, K., Ishikawa, T., Yamaguchi, T.: Inflow into saccular cerebral aneurysms at arterial bends. *Annals of Biomedical Engineering* **36**(9), 1489–95 (2008)
19. Jou, L., Lee, D., Morsi, H., Mawad, M.: Wall shear stress on ruptured and unruptured intracranial aneurysms at the internal carotid artery. *American Journal of Neuroradiology* **29**(9), 1761–7 (2008)
20. Kraysenbuehl, H., Huber, P., Yasargil, M.G.: *Kraysenbuehl/yasargil cerebral angiography*. Thieme Medical Publishers, 2nd ed. (1982)
21. Moyle, K., Antiga, L., Steinman, D.A.: Inlet conditions for image-based CFD models of the carotid bifurcation: is it reasonable to assume fully developed flow? *Journal of Biomechanical Engineering* **128**, 371–379 (2006)
22. Nichols, W.W., O'Rourke, M.F.: *McDonald's blood flow in arteries: theoretical, experimental and clinical principles*. A Hodder Arnold Publication (1998)
23. Nixon, A., Gunel, M., Sumpio, B.: The critical role of hemodynamics in the development of cerebral vascular disease. *Journal of Neurosurgery* **112**(6), 1240–53 (2010)
24. Passerini, T.: *Computational hemodynamics of the cerebral circulation: multiscale modeling from the circle of willis to cerebral aneurysms*. thesis, Politecnico di Milano (2009)
25. Piccinelli, M., Bacigaluppi, S., Boccardi, E., Ene-Iordache, B., Remuzzi, A., Veneziani, A., Antiga, L.: Geometry of the ica and recurrent patterns in location, orientation and rupture status of lateral aneurysms: an image-based computational study. *Neurosurgery* **68**(5), 1270–1285 (2011)
26. Piccinelli, M., Veneziani, A., Steinman, D.A., Remuzzi, A., Antiga, L.: A framework for geometric analysis of vascular structures: applications to cerebral aneurysms. *IEEE Trans Med Imag* **28**(8), 1141–55 (2009)
27. R Development Core Team: *R: A Language and Environment for Statistical Computing*. R Foundation for Statistical Computing, Vienna, Austria (2010)
28. Raghavan, M., Ma, B., R.E., H.: Quantified aneurysm shape and rupture risk. *Journal of Neurosurgery* **102**(2), 355–62 (2005)
29. Ramsay, J.O., Silverman, B.W.: *Functional Data Analysis*. Springer (2005)

30. Sangalli, L.M., Secchi, P., Vantini, S., Veneziani, A.: A case study in exploratory functional data analysis: Geometrical features of the internal carotid artery. *J. Am. Stat. Assoc.* **104**(485), 37–48 (2009)
31. Sangalli, L.M., Secchi, P., Vantini, S., Veneziani, A.: Efficient estimation of three-dimensional curves and their derivatives by free knot regression splines, applied to the analysis of inner carotid artery centrelines. *Journal of the Royal Statistical Society Ser. C* **58**(3), 285–306 (2009)
32. Sangalli, L.M., Secchi, P., Vantini, S., Vitelli, V.: Joint clustering and alignment of functional data: an application to vascular geometries. In: *Joint Statistical Meetings Proceedings*, pp. 4034–4047 (2010)
33. Sangalli, L.M., Secchi, P., Vantini, S., Vitelli, V.: K-means alignment for curve clustering. *Computational Statistics and Data Analysis* **54**, 1219–1233 (2010)
34. Sato, K., Imai, Y., Ishikawa, T., Matsuki, N., Yamaguchi, T.: The importance of parent artery geometry in intra-aneurysmal hemodynamics. *Medical Engineering & Physics* **30**(6), 774–82 (2008)
35. Sforza, D., Putman, C., Cebal, J.R.: Hemodynamics of cerebral aneurysms. *Annu Rev Fluid Mech* **41** (2009)
36. Xiang, J., Natarajan, S., Tremmel, M., Ma, D., Mocco, J., Hopkins, L., Siddiqui, A., Levy, E., Meng, H.: Hemodynamic-morphologic discriminants for intracranial aneurysm rupture. *Stroke* **42**(1), 144–52 (2011)
37. Zienkiewicz, O., Taylor, R., Too, J.: Reduced integration technique in general analysis of plates and shells. *Int. J. Numer. Methods Eng.* **3**(2), 275–290 (1971)

MOX Technical Reports, last issues

Dipartimento di Matematica “F. Brioschi”,
Politecnico di Milano, Via Bonardi 9 - 20133 Milano (Italy)

- 19/2011 PASSERINI, T.; SANGALLI, L.; VANTINI, S.; PICCINELLI, M.; BACIGALUPPI, S.; ANTIGA, L.; BOCCARDI, E.; SECCHI, P.; VENEZIANI, A.
An Integrated Statistical Investigation of the Internal Carotid Arteries hosting Cerebral Aneurysms
- 18/2011 BLANCO, P.; GERVASIO, P.; QUARTERONI, A.
Extended variational formulation for heterogeneous partial differential equations
- 17/2011 QUARTERONI, A.; ROZZA, G.; MANZONI, A.
Certified Reduced Basis Approximation for Parametrized Partial Differential Equations and Applications
- 16/2011 MESIN, L; AMBROSI, D.
Spiral waves on a contractile tissue
- 15/2011 ARGIENTO, R.; GUGLIELMI, A.; SORIANO J.
A semiparametric Bayesian generalized linear mixed model for the reliability of Kevlar fibres
- 14/2011 ANTONIETTI, P.F.; MAZZIERI, I.; QUARTERONI, A.; RAPETTI, F.
Non-Conforming High Order Approximations for the Elastic Wave Equation
- 13/2011 LOMBARDI, M.; PAROLINI, N.; QUARTERONI, A.; ROZZA, G.
Numerical simulation of sailing boats: dynamics, FSI, and shape optimization
- 12/2011 MIGLIO E.; CUFFARO M.
Tectonic evolution at mid-ocean ridges: geodynamics and numerical modeling
- 11/2011 FORMAGGIA, L.; MINISINI, S.; ZUNINO, P.
Stent a rilascio di farmaco: una storia di successo per la matematica applicata
- 10/2011 ZUNINO, P.; VESENTINI, S.; PORPORA, A.; SOARES, J.S.; GAUTIERI, A.; REDAELLI, A.
Multiscale computational analysis of degradable polymers